forests

MDPI

Article

Evaluation of Accuracy in Estimating Diameter at Breast Height Based on the Scanning Conditions of Terrestrial Laser Scanning and Circular Fitting Algorithm

Yongkyu Lee and Jungsoo Lee *

Department of Forest Management, Kangwon National University, Chuncheon 24341, Republic of Korea; kong445566@kangwon.ac.kr
* Correspondence: jslee72@kangwon.ac.kr

Abstract: A growing societal interest exists in the application of lidar technology to monitor forest resource information and forestry management activities. This study examined the possibility of estimating the diameter at breast height (DBH) of two tree species, *Pinus koraiensis* (*PK*) and *Larix kaempferi* (*LK*), by varying the number of terrestrial laser scanning (TLS) scans (1, 3, 5, 7, and 9) and DBH estimation methods (circle fitting [CF], ellipse fitting [EF], circle fitting with RANSAC [RCF], and ellipse fitting with RANSAC [REF]). This study evaluates the combination that yields the highest estimation accuracy. The results showed that for *PK*, the lowest RMSE of 0.97 was achieved when REF was applied to the data from nine scans after noise removal. For *LK*, the lowest RMSE of 1.03 was observed when applying CF to the data from seven scans after noise removal. Furthermore, ANOVA revealed no significant difference in the estimated DBH from nine scans when more than three scans were used for CF and RCF and more than five for EF and REF. These results are expected to be useful in establishing efficient and accurate DBH estimation plans using TLS for forest resource monitoring.

Keywords: LiDAR; TLS; DBH; RANSAC; circular fitting; circle fitting; ellipse fitting

Citation: Lee, Y.; Lee, J. Evaluation of Accuracy in Estimating Diameter at Breast Height Based on the Scanning Conditions of Terrestrial Laser Scanning and Circular Fitting Algorithm. *Forests* **2024**, *15*, 313. https://doi.org/10.3390/f15020313

Academic Editors: Zhenyang Hui, Penggen Cheng, Bo Liu, Mark Vanderwel and Cate Macinnis-Ng

Received: 22 December 2023
Revised: 29 January 2024
Accepted: 4 February 2024
Published: 7 February 2024

1. Introduction

Traditional monitoring of forest resources for the construction of forest structural parameters typically involves in situ measurements using diameter tapes, calipers, and hypsometers [1]. In particular, diameter at breast height (DBH) is a fundamental parameter for calculating forest biomass and is used in various forest resource-related models, including stem taper, growth prediction, and height estimation [2–4].

Research related to DBH measurement has been conducted on comparisons of measurement results based on measurement height and tools, such as calipers and diameter tapes, as well as analyses of differences due to field crews [5–7]. Since the 2000s, with the advancement of remote sensing techniques, data collection using various platforms has become feasible, leading to diverse studies on DBH estimation modeling using satellite imagery, drone imagery, and 'light detection and ranging (LiDAR)' [8,9]. In particular, LiDAR technology, which is capable of acquiring high-resolution three-dimensional data, has been extensively researched for extracting information on forest structural parameters [10].

Research on DBH estimation using LiDAR utilizes data collected from various platforms and sensors including terrestrial laser scanning (TLS), mobile laser scanning (MLS), and airborne laser scanning (ALS). ALS has been commonly used for decades, but recently, there has been concurrent research on the utilization of TLS and MLS for ground-based data collection. Because it involves data acquisition from aircraft, ALS allows for efficient data collection; however, its low point density limits its analysis of forest structures. However, TLS and MLS collect data from the lower parts of a forest, making them more suitable for analyzing forest structures. MLS, utilizing localization algorithms (e.g., simultaneous localization and mapping), is more effective in covering large areas and addressing

occlusions owing to its ability to move while scanning. However, its accuracy is lower than that of TLS owing to cumulative errors in scanner positioning and movement. TLS, being stationary, can gather high-density and accurate point data on clouds compared to other platforms. However, occlusions can occur owing to terrain and other obstructions, necessitating adjustments in the number and positions of scans to effectively collect data on point clouds [11,12].

In particular, TLS enables high-accuracy DBH estimation based on dense and precise point cloud data, compared to LiDAR systems on other platforms [13]. Consequently, numerous studies have applied various algorithms using TLS to estimate DBH, such as the Hough transform, circle fitting algorithm, ellipse fitting algorithm, linear least square circle fitting, nonlinear least square circle fitting, minimum bounding box method, centroid method, and maximum distance method. These studies have also proposed new algorithms in this field [14–19]. Additionally, the random sample consensus (RANSAC) algorithm was presented as an effective method for eliminating the influence of noise [20]. The accuracy of DBH estimation using TLS can vary under different conditions. According to previous research, higher slopes may result in lower accuracy of DBH estimation [21]. Moreover, because TLS operates from a fixed point and rotates to acquire data, high stand density and uneven vertical distribution can lead to significant occlusions [22,23]. Consequently, the number of TLS scans significantly impacts data quality. Scanning methods are primarily categorized into single-scanning and multi-scanning, depending on the number of scans. Single-scanning was typically conducted at the center of the plot. Consequently, although data acquisition and preprocessing are rapid, this method is vulnerable to occlusions caused by the terrain and objects [24]. Multi-scanning involves scanning more than twice and aligning the collected data for acquisition. In multi-scanning, there is a trade-off relationship in which an increased scanning frequency leads to higher costs but also improves accuracy [21].

Previous studies have primarily focused on applying various algorithms to single-point clouds acquired in forest environments. However, these approaches often fail to thoroughly examine the relationship between the number of TLS scans, point cloud quality, and DBH estimation accuracy. Therefore, this study aimed to analyze the patterns of accuracy variation relative to the number of TLS scans in the same study area. Additionally, the impact of the presence and treatment of noise and various DBH estimation methods on accuracy was investigated, intending to contribute to the development of forest point cloud strategies for DBH estimation.

2. Materials and Methods

In this study, point clouds were collected using the TLS. The datasets were created from data scanned one, three, five, seven, and nine times following the alignment and ground control points (GCP) correction processes. The point cloud constructed for each scanning frequency was processed using a Cloth Simulation Filter (CSF) algorithm to extract ground points and construct the mesh data of the terrain. Subsequently, the distance between the mesh and points was calculated to extract the DBH point cloud at breast height (ranging from 1.15 to 1.25 m). The location of each tree was determined using the position coordinates collected using the Real-Time Kinematic (RTK) system during the field surveys. For each tree, DBH was estimated and evaluated using circle fitting (CF), ellipse fitting (EF), RANSAC circle fitting (RCF), and RANSAC ellipse fitting (REF) on the respective DBH point cloud. Finally, for each tree, the Completeness of the Stem Point Cloud (CPC), Field DBH, Point Density, and Slope were calculated, and their relationship with bias was analyzed (Figure 1).

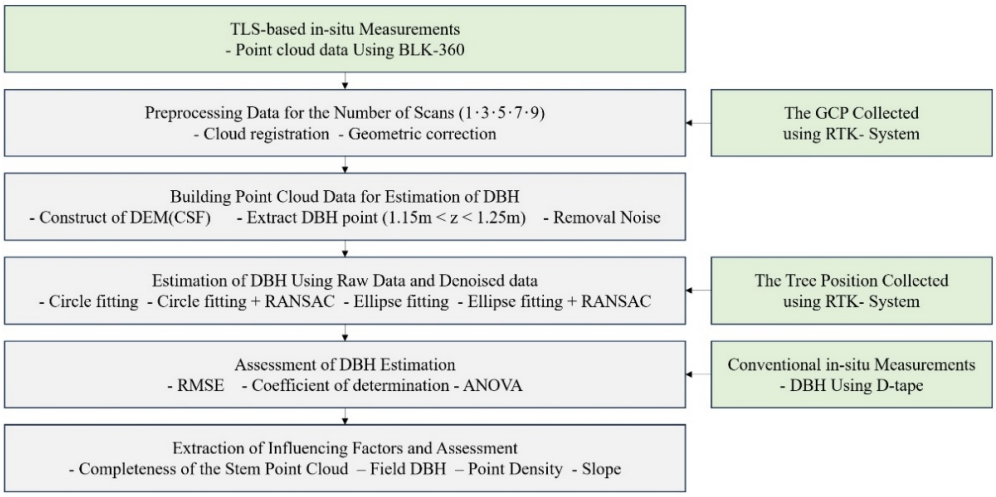

Figure 1. Workflow Diagram of the Research Methodology for DBH Estimation Using Terrestrial Laser Scanning (TLS).

2.1. Study Area

This research was conducted in Kangwon-do within the academic forest of Kangwon National University. Five plots each for *Pinus koraiensis* (*PK*) and five for *Larix kaempferi* (*LK*) were installed. The plots were configured as circles with a radius of 11.3 m. The *PK* and *LK* plots were artificial forests of the fifth age class, with 185 *PK* trees and 78 *LK* trees distributed across the five plots. The average slope of the five plots was approximately 21° for *PK* and 40° for *LK*, indicating variation in stand density and slope between species. Additionally, *LK* had a lower stand density than *PK*, and owing to the characteristics of the species, a higher amount of light was passing through the canopy, leading to well-developed understory vegetation [25] (Figure 2).

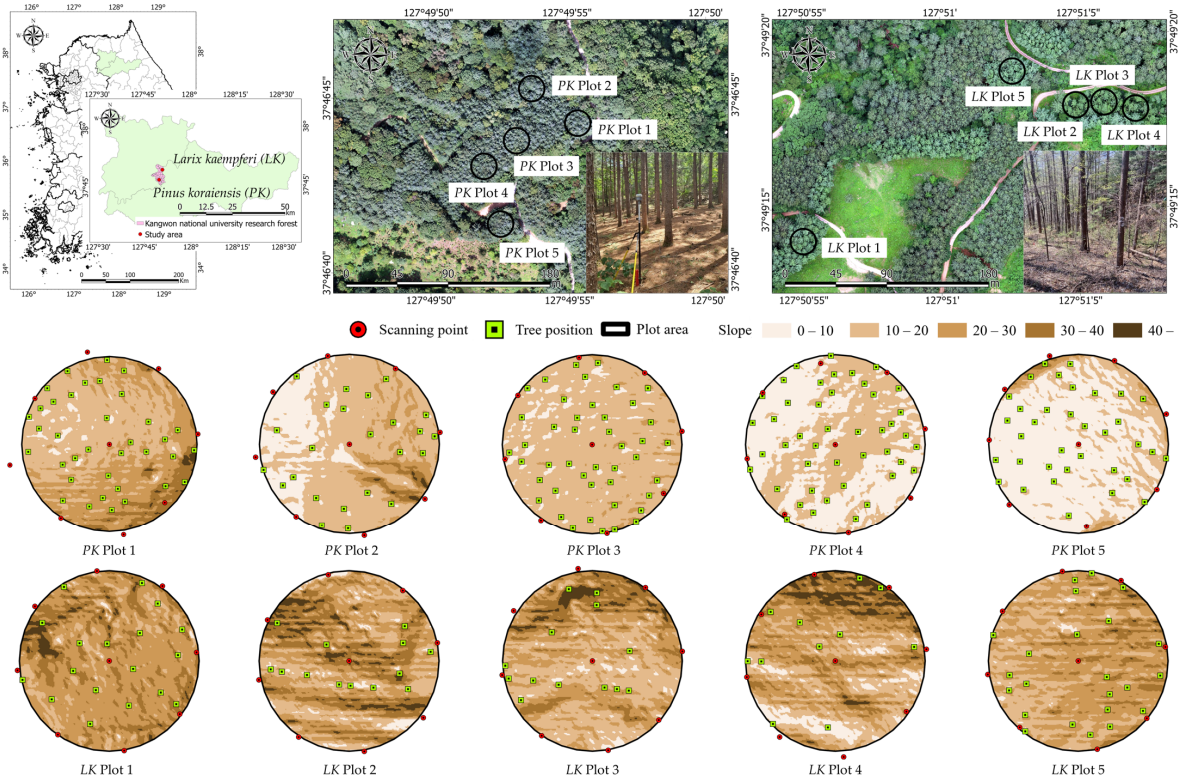

Figure 2. Location map and drone orthophoto of the study area, along with schematics showing slope, individual tree positions, and scanning locations for each research plot.

2.2. Data Acquisition and Preprocessing

2.2.1. Field Survey for DBH and Individual Tree Locations

During the field survey, data on the locations and DBH of individual trees were collected. The DBH was measured using a diameter tape at a height of 1.2 m from the ground in accordance with the standards of the National Forest Resources Survey of South Korea [26]. The locations of individual trees were determined using an RTK system composed of two R12i units (Trimble Inc., Westminster, CO, USA). One of the two units was installed in a cleared area on a forested road and served as the base station. The other unit, which was used as a rover, was employed within the forest to acquire points in close proximity to each tree. The location of individual trees acquired using the RTK system was used to match the estimated Diameter at Breast Height (DBH) from the LiDAR data with the Field DBH measured using a diameter tape. The average DBH was 27.4 cm at *PK* and 32.3 cm at *LK* (Table 1).

Table 1. The statistics of each plot using conventional in situ measurements.

Species	Plot	Number of Trees (*n*)	Stem Density (Stems/ha)	DBH (cm)				Basal Area (m^2/ha)
				Min	Max	Mean	Std	
PK	1	37	925	12.9	43.0	27.6	8.2	1258
	2	25	625	12.5	50.3	30.0	8.3	925
	3	44	1100	15.0	47.0	26.5	7.0	1438
	4	44	1100	12.0	42.0	25.9	6.0	1408
	5	35	875	16.0	42.8	28.5	6.0	1230
	Total	185	925	12.0	50.3	27.4	7.1	1252
LK	1	18	450	22.3	38.2	31.2	4.8	692
	2	13	325	20.1	40.5	31.3	6.5	501
	3	13	325	16.9	46.5	33.2	8.6	532
	4	11	275	23.9	47.5	37.3	8.7	506
	5	23	575	16.2	42.8	31.0	7.5	879
	Total	78	390	16.2	47.5	32.3	7.3	622

2.2.2. Data Collection and Preprocessing

Data collection using TLS includes scanning for point cloud acquisition and establishing GCPs for georeferencing. The collection of point cloud data was conducted using the BLK 360 (Leica Geosystems AG., Heerbrugg, Switzerland). The BLK 360 is mounted on a tripod for use. It can complete scanning within 5 min from a single position and accurately collect data within a radius of 10–15 m. The specifications of the BLK 360 include a shooting range of 0.6–60 m, a point measurement rate of over 360,000 points per second, and a ranging accuracy of 4 mm at 10 m [27,28]. The scanning positions were set up once at the center of the standard plot and at eight directional points located 11.3 m from the center (Figure 3). Each scanning location was determined using a tape measure and a compass from the center of the plot, and stakes were installed for easy identification at each location. In addition, the positions of the installed stakes were recorded using an RTK system to acquire the GCPs.

Preprocessing of the TLS data was performed in the order of alignment, followed by GCP correction. Registration was performed on data captured 1, 3, 5, 7, and 9 times to compare the results of DBH estimation according to the number of scans. Data from 2, 4, 6, and 8 scans were excluded from the analysis owing to the asymmetric positioning of the scanning locations when including the central position. The root mean square error (RMSE) for all registration processes was maintained below 5 mm. The scanning positions used for each number of scans correspond to those shown in Figure 3. The GCP correction was performed individually for the point cloud constructed for each number of scans, matching the stakes identifiable in each point cloud to the GCPs. All the GCP correction processes were completed with an RMSE of less than 5 cm. Finally, the noise points located below the ground and points situated beyond 13 m from the central coordinates (x and y) and outside

the plot were removed. Cyclone (2023.0.2) software was used for alignment, whereas cloud computing was employed for geometric correction and point removal.

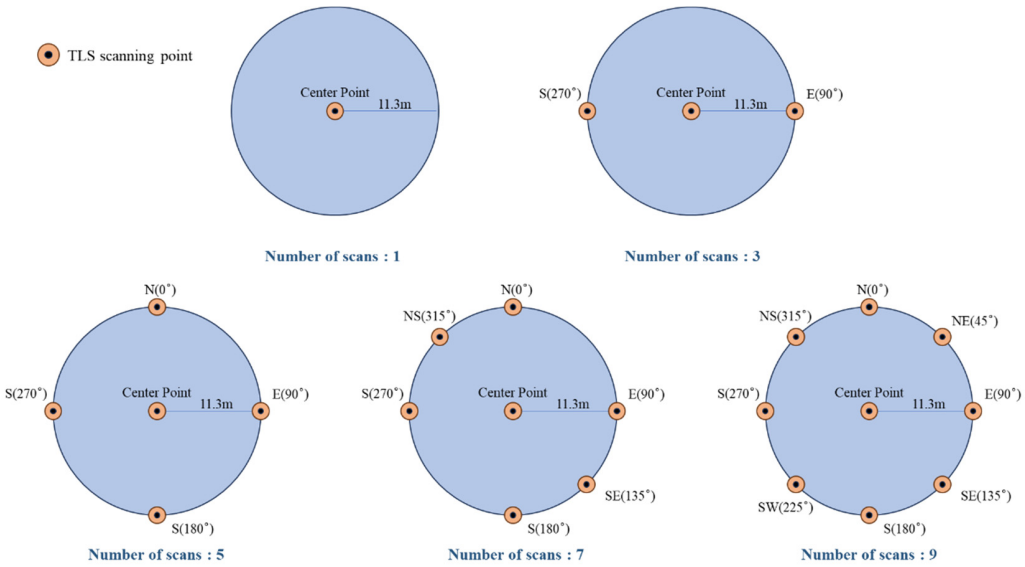

Figure 3. Scanning positions of the TLS according to the number of scans.

2.2.3. Noise Point Removal for DBH Estimation

The constructed point clouds contain points distributed across the understory vegetation and canopy, which are unnecessary for DBH estimation and necessitate the preprocessing of these points. Firstly, the Cloth Simulation Filter (CSF) algorithm was applied to extract ground points, and the extracted ground points were used to construct terrain mesh information [29,30]. The parameters for the CSF filter were set as follows: cloth resolution at 0.1, max iterations at 900, and classification threshold at 0.1. The ground mesh constructed using CSF was set above the actual ground at locations where individual trees existed, but ground points did not. To address this, the smooth mesh tool was utilized to create a uniform ground mesh. The parameters for the smooth mesh were set at 20 iterations and a smoothing factor of 0.2. Furthermore, the distance of each point from the ground was calculated, and considering the measurement height for DBH, points located at a distance of 1.15 m–1.25 m from the ground were extracted. The extracted points were defined as 'raw data'. 'Raw data' includes branches and understory vegetation that could interfere with the estimation of DBH [31]. Subsequently, noise points that were unnecessary for the DBH estimation were removed through visual inspection. The data from which these points were removed was defined as 'denoised data' and used to construct the DBH point cloud (Figure 4). This process was performed using cloud compare (v2.13 beta) software.

2.3. Estimation and Evaluation of DBH Using Circular Fitting

Algorithm-based circular fitting, as opposed to manual measurement of DBH, eliminates subjectivity and offers high reproducibility when the same data are used [32]. Therefore, the least squares method for CF and EF algorithms for DBH estimation was applied in this study [33]. The least squares method seeks the optimal solution where the sum of the squared distances between the given points and the drawn circle is minimized. Additionally, the RANSAC algorithm, known for its high performance in noisy data environments, was applied to each fitting algorithm, resulting in four DBH estimation outcomes, including RCF and REF. The optimal solutions for CF and EF were estimated using the x, y coordinates of points within 30 cm from the center of individual trees and the normal equation.

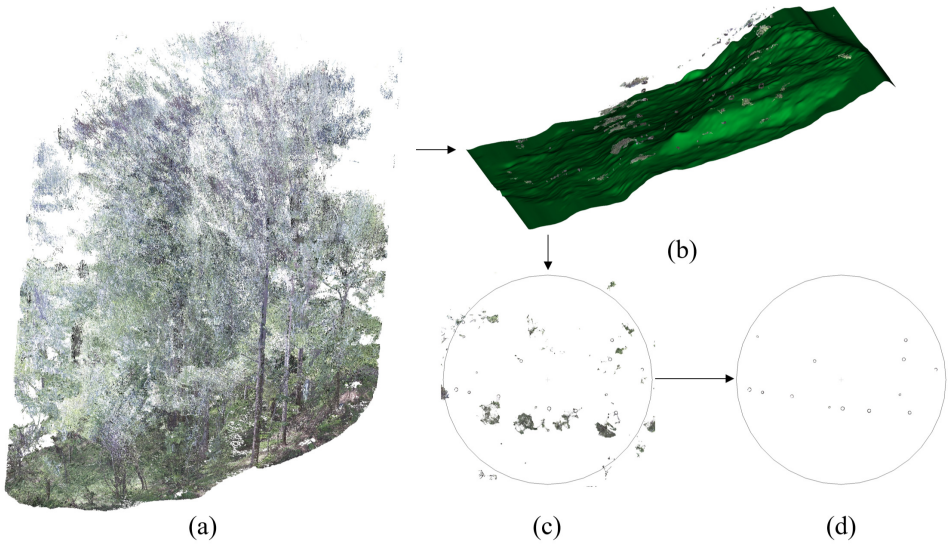

Figure 4. Constructing point clouds for DBH: (**a**) a scanned plot using TLS; (**b**) construction of the ground mesh using CSF and extracted points at 1.15–1.25 m height range from the ground; (**c**) top view of constructed DBH point cloud (raw data); (**d**) top view of denoised DBH point cloud (denoised data).

The RANSAC algorithm is a method for predicting noise removal from the given data [34]. The RANSAC algorithm procedure is primarily divided into the hypothesis phase and the verification phase, and it operates by iterating through these two stages. The hypothesis phase involves extracting n data points from the entire dataset and applying a prediction model, whereas the verification phase evaluates the applied results and stores the model with the highest performance. In this study, the hypothesis phase involved randomly selecting 10 points to apply the CF and EF. The verification phase was evaluated based on the number of points in the entire dataset whose distances from the estimated circle were below the threshold (0.6 cm). These two phases were repeated 100 times, and the circle with the highest number of points within the threshold was selected [20]. The threshold was set based on the error range of the BLK360 when used at a shooting distance of 10 m.

The evaluation of the DBH estimation results involved checking the possibility of estimating DBH according to the circular fitting method and the number of scanning sessions. Cases were defined as unfeasible for estimation when the circular fitting method yielded negative radius values or when the DBH was estimated to be outside the 6–60 cm range. Accuracy was evaluated by comparing the DBH estimated using the circular fitting method with the Field DBH. This comparison considered factors such as noise removal, tree species, and number of scans. Subsequently, the RMSE and R^2 were calculated based on these comparisons. Additionally, to determine the optimal number of scans for each circular fitting method, analysis of variance (ANOVA) was conducted. This analysis tested for significant differences at the 0.05 level in the mean absolute values of the bias between the number of scans for each circular fitting method. Furthermore, post hoc tests were performed to examine whether there were significant differences in the mean absolute values of bias when comparing one, three, five, and seven scans against the highest number of scans, which was nine.

2.4. Construction and Evaluation of Influencing Factors on DBH Estimation

The influencing factors were CPC, Point Density, Field DBH, and Slope. Because the TLS is scanned from a single location, it is difficult to collect complete data for a plot owing to occlusion by terrain and objects. Therefore, in the case of a single scan or an insufficient number of scans, the point cloud for DBH is formed as an incomplete circle. The Circular fitting method can estimate DBH with an incomplete circle. However, the

incompleteness of a circle can affect DBH estimation [35]. Consequently, the CPC was selected as the influencing factor. The CPC involves constructing the central point of each tree and calculating the angle with all points of the DBH point cloud, rounding off to the nearest degree. Subsequently, the CPC was calculated in percentage terms by removing duplicate values of the calculated angles and dividing the count of unique values by 360.

The point density increased as the distance between the LiDAR and subject decreased, and additional scanning was conducted at various locations. Point density was added as an influencing factor, considering the relationship between the scanning locations and positions of individual trees [21]. Point density was calculated by dividing the number of points in the DBH point cloud by the length of the circular arc, resulting in the number of points per centimeter. The length of the circular arc was calculated using the computed CPC.

Field DBH and Slope were selected as influencing factors based on prior research that indicated that DBH and slope affect estimation accuracy [35,36]. The slope was calculated by constructing a 1-m buffer zone around the central point of the DBH point cloud and computing the average of the pixels located within the buffer zone. The slope for each plot was determined using the digital elevation model (DEM) constructed for that plot. The DEM was based on point cloud data collected from nine scans. Utilizing the constructed ground mesh, a DEM with a resolution of 10 cm was created (Figure 5). The CPC and Point Density were calculated using Python (3.7.2), while Slope was constructed using the Cloud Compare and ArcGIS Pro (3.0.2) programs.

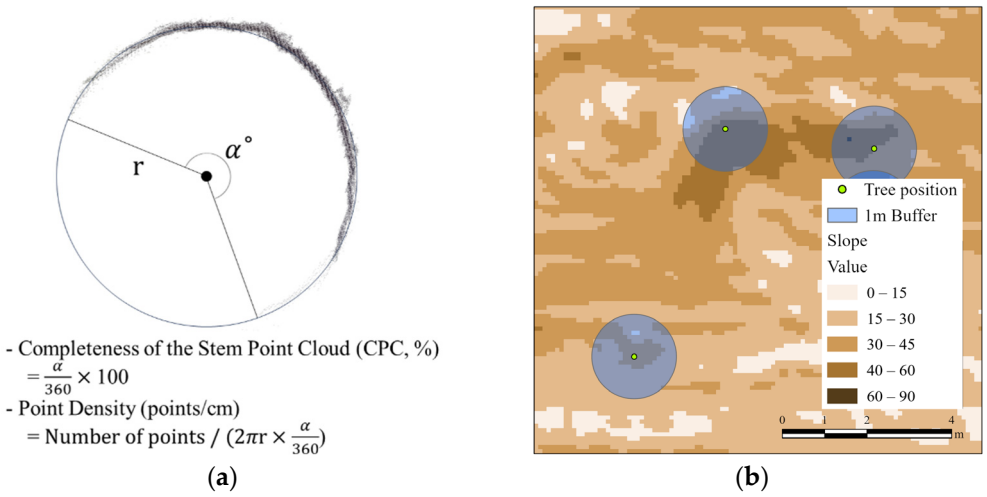

Figure 5. Extraction of influencing factors: (**a**) examples of calculating the 'completeness of the stem point cloud (CPC, %)' and 'point density'; (**b**) calculating average slope values within a 1-m radius around individual tree.

3. Results and Discussion

3.1. Evaluation of the Possibility of DBH Estimation Based on the Circular Fitting Method and Number of Scans

In *PK*, DBH estimation was possible for all individual trees using five scans. The number of trees that could be estimated was the same for both denoised and raw data. In contrast, for *LK*, DBH estimation was possible for all individual trees using the three scans, except when EF was applied to the raw data (Table 2). When a single scan was conducted, the number of trees for which DBH estimation was possible was the same for both CF and RCF. In addition, the distribution was higher for CF and RCF than for REF and EF. DBH estimation using CF and RCF was possible even when a small number of points were collected. However, with EF and REF, when a few points were collected, the DBH was estimated to be less than 6 cm, rendering the estimation infeasible (Figure 6a). In contrast, in *LK*, with abundant understory vegetation, using EF on raw data from nine scans led to an overestimation in some cases. Specifically, two individual trees were estimated to have DBHs exceeding 60 cm owing to noise points, rendering the DBH estimation unfeasible

(Figure 6b). Consequently, to estimate the DBH for all individual trees, it is necessary to consider the environmental conditions of the study area and the circular fitting algorithm. To estimate the DBH of all individual trees in each plot, noise points were removed and at least five scanning sessions were performed. The CF was more suitable than the EF for data from fewer than five scans. Additionally, because EF is sensitive to noise points, it is essential to include a process for removing these points or to consider the application of the RANSAC algorithm.

Table 2. Number of trees for which DBH estimation was possible based on noise removal status, number of scans, and circular fitting algorithm.

Species		*PK* (*n* = 185)					*LK* (*n* = 78)				
Number of Scans		1	3	5	7	9	1	3	5	7	9
Raw data	CF	174	184	185	185	185	74	78	78	78	78
	RCF	174	184	185	185	185	74	78	78	78	78
	EF	164	184	185	185	185	65	74	76	76	76
	REF	168	184	185	185	185	72	78	77	76	78
Denoised data	CF	174	184	185	185	185	74	78	78	78	78
	RCF	174	184	185	185	185	74	78	78	78	78
	EF	164	184	185	185	185	71	78	78	78	78
	REF	168	184	185	185	185	72	78	78	78	78

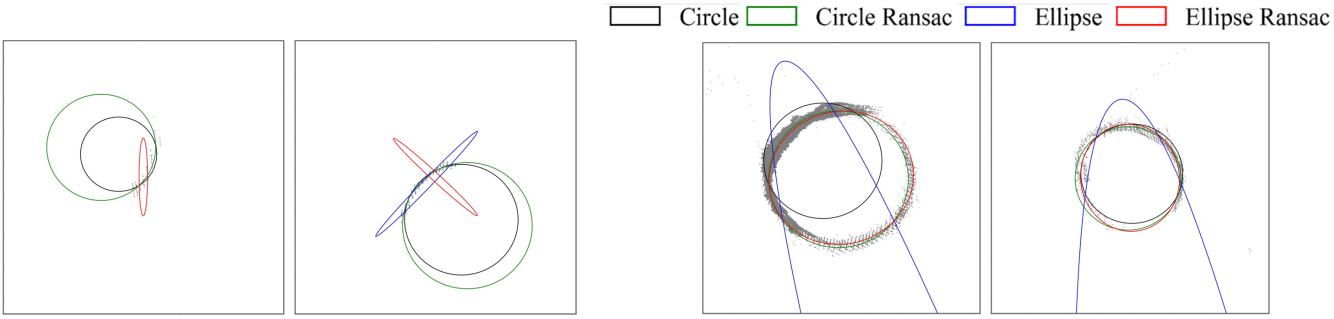

Figure 6. Cases of DBH estimation using the circular fitting method being unfeasible: (**a**) a case of underestimation below 6 cm using EF and REF in a single scan data; (**b**) a case of overestimation above 60 cm using EF in the data of nine scans.

3.2. Accuracy Evaluation of DBH Estimation

For both tree species, the highest accuracy was achieved when the REF was applied to the data scanned seven times, resulting in an RMSE of 1.01 *PK* and 1.12 *LK*. In the denoised data, the highest accuracy for *PK* was observed when REF was applied to data scanned nine times, with an RMSE of 0.97. For *LK*, the highest accuracy was achieved using CF on data scanned seven times, resulting in an RMSE of 1.03. The aforementioned RMSE values were distributed similarly to the range of 0.5 to 1.6 cm for RMSE obtained in previous studies on DBH estimation [13,37–39] (Table 3).

As a result of estimating DBH using a single scan, a difference in accuracy was observed between CF and EF. In single-scanning data, the RMSE of EF was approximately 1.3 to 3.7 times higher than that of CF. Therefore, CF is deemed more suitable for single-scanning data. In contrast, in the multi-scanning data, the RMSE decreased for both the raw and denoised data as the number of scans increased. In particular, the accuracies of EF and REF improved significantly as the number of scans increased. In four cases based on noise removal status and tree species, REF achieved the lowest RMSE in three of the cases. Accordingly, EF is more significantly influenced by the number of scans than CF. EF

requires optimization of more variables, such as the center point, major axis, minor axis, and rotation angle, compared with CF during the fitting process. Therefore, sufficient data acquisition is necessary for accurate DBH estimation using EF.

Table 3. Evaluation results of accuracy by tree species and number of scans according to noise removal status and circular fitting method.

Species			*PK*					*LK*				
Number of Scans			1	3	5	7	9	1	3	5	7	9
Raw data	CF	RMSE	3.27	1.53	1.55	1.55	1.46	3.21	2.92	2.23	2.59	1.64
		r^2	0.81	0.96	0.96	0.96	0.96	0.83	0.86	0.91	0.89	0.96
	RCF	RMSE	2.95	1.59	1.85	1.80	1.79	2.54	2.02	1.57	1.33	1.28
		r^2	0.84	0.95	0.94	0.94	0.94	0.89	0.94	0.96	0.97	0.98
	EF	RMSE	4.71	2.24	1.54	1.45	1.32	7.12	3.53	1.92	1.90	1.72
		r^2	0.70	0.91	0.96	0.96	0.97	0.53	0.78	0.93	0.93	0.95
	REF	RMSE	4.58	1.75	1.17	1.01	1.03	6.06	2.72	1.38	1.12	1.33
		r^2	0.67	0.94	0.98	0.99	0.99	0.59	0.89	0.98	0.99	0.98
Denoised data	CF	RMSE	3.08	1.12	1.10	1.06	1.03	1.68	1.25	1.14	1.03	1.09
		r^2	0.84	0.98	0.98	0.99	0.99	0.95	0.99	0.99	0.99	0.99
	RCF	RMSE	2.69	1.29	1.31	1.25	1.18	2.00	1.57	1.35	1.30	1.13
		r^2	0.87	0.97	0.98	0.98	0.98	0.93	0.97	0.98	0.98	0.99
	EF	RMSE	4.13	1.56	1.27	1.11	1.02	6.19	2.65	1.11	1.09	1.10
		r^2	0.78	0.96	0.98	0.99	0.99	0.63	0.90	0.99	0.99	0.99
	REF	RMSE	4.05	1.73	1.16	1.20	0.97	6.52	2.46	1.22	1.84	1.26
		r^2	0.74	0.94	0.98	0.98	0.99	0.53	0.91	0.98	0.95	0.98

However, in some cases, the RMSE increases with the number of scans. Such cases were predominantly observed when the raw data were used. For example, when using raw data from single-scanning data, there were no noise points, allowing all four circular fitting methods to correctly estimate the DBH. However, as the number of scans increased, noise points were progressively added, leading to gradually larger errors in DBH estimation by CF and EF. Notably, EF was more significantly affected by noise points than CF (Figure 7).

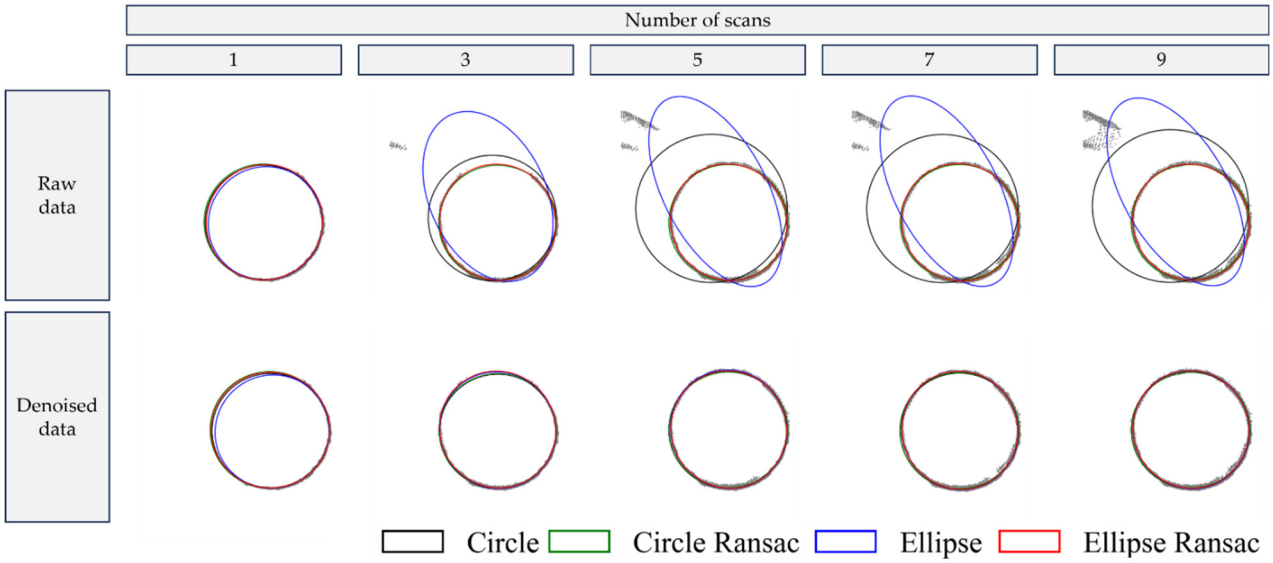

Figure 7. Results of applying circular fitting algorithms with increasing number of scans in raw and denoised data (*LK*, Plot 3, No. 13).

Using fitting methods where the RANSAC algorithm was applied, it was possible to accurately estimate the DBH, even in the presence of some noise points. Consequently, in the cases mentioned above, as the number of scans increased, the point cloud from understory vegetation and branches around the individual trees affected the accuracy of DBH estimation. It is considered appropriate to improve this by applying the RANSAC algorithm or using denoised data. However, in data without noise, the application of the RANSAC algorithm sometimes led to reduced accuracy. This is because the RANSAC algorithm randomly samples some data for fitting, which can result in a biased algorithm focused on a subset of data. The number of samples is a crucial parameter in the RANSAC algorithm; it can lead to bias towards a subset of the data if it is too small and an increased likelihood of including surrounding noise data if it is too high. Therefore, depending on the acquired data and fitting algorithm used, there is a need to evaluate whether to apply the RANSAC algorithm and review its parameters.

3.3. Optimal Number of Scans for Estimating DBH Using TLS

ANOVA was conducted for each of the four circular fitting methods to evaluate the impact of the number of scans on accuracy. The analysis results showed that the absolute values of bias differed significantly according to the number of scans in all the Circular Fitting methods. The F-statistic for the CF method was approximately 12.9, whereas that for the EF method was much higher at 81.9. This indicates that the EF method is more sensitive than the CF method to changes in the number of scans with respect to the absolute value of the CF method. Additionally, when the RANSAC algorithm was applied to both the CF and EF methods, the F-statistic decreased, indicating that the variation in bias due to the number of scans was reduced by the RANSAC algorithm. These results suggest that the RANSAC algorithm can mitigate the impact of the number of scans on the bias (Table 4).

Tamhane's T2 post hoc test was used to verify the changes in the absolute values of bias according to the number of scans. The absolute values of the bias obtained from nine scans were compared with those obtained from one, three, five, and seven scans. Significant differences were observed between the absolute values of bias for one and nine scans in CF and RCF, and between one, three, and nine scans for EF and REF. Consequently, three scans for CF and RCF and five scans for EF and REF were sufficient to produce bias estimates that were as accurate as those from nine scans, without any significant difference. This implies that reliable DBH estimates can be obtained even with fewer scans. Therefore, from an efficiency standpoint, it is advisable to conduct three scans for CF and RCF, and five scans for EF and REF (Table 5).

Table 4. ANOVA analysis results of the number of scans for each circular fitting using denoised data.

Dependent Variable		Sum of Squares	df	Mean Square	F	Sig.
Absolute Deviation of CF	Between Groups	30.43	4	7.61	12.94	0.00
	Within Groups	752.27	1280	0.59		
	Total	782.70	1284			
Absolute Deviation of RCF	Between Groups	24.07	4	6.02	7.21	0.00
	Within Groups	1067.70	1280	0.83		
	Total	1091.78	1284			
Absolute Deviation of EF	Between Groups	1021.90	4	255.48	81.95	0.00
	Within Groups	3990.38	1280	3.12		
	Total	5012.28	1284			
Absolute Deviation of REF	Between Groups	604.61	4	151.15	53.44	0.00
	Within Groups	3620.47	1280	2.83		
	Total	4225.08	1284			

Table 5. Determining the optimal number of scans using Tamhane's T2 post hoc test.

Dependent Variable	Number of Scanning (I)	Number of Scanning (J)	MeanDifference (I–J)	Std. Error	Sig.	95% Confidence Interval	
						Lower Bound	Upper Bound
Absolute Deviation of CF	9	1	−0.42 *	0.08	0.00	−0.64	−0.21
		3	−0.11	0.06	0.52	−0.29	0.06
		5	−0.04	0.06	1.00	−0.22	0.14
		7	−0.00	0.06	1.00	−0.17	0.16
Absolute Deviation of RCF	9	1	−0.39 *	0.09	0.00	−0.63	−0.15
		3	−0.17	0.07	0.20	−0.37	0.04
		5	−0.06	0.07	0.99	−0.27	0.15
		7	−0.05	0.07	1.00	−0.25	0.15
Absolute Deviation of EF	9	1	−2.41 *	0.23	-	−3.07	−1.74
		3	−0.36 *	0.11	0.01	−0.66	−0.06
		5	−0.09	0.07	0.84	−0.28	0.09
		7	−0.03	0.06	1.00	−0.20	0.14
Absolute Deviation of ECF	9	1	−1.86 *	0.21	0.00	−2.47	−1.26
		3	−0.42 *	0.10	0.00	−0.71	−0.13
		5	−0.04	0.06	1.00	−0.22	0.14
		7	−0.07	0.08	0.99	−0.29	0.15

* The mean difference is significant at the 0.05 level.

3.4. Evaluation of Factors Affecting the Accuracy of DBH Estimation

The average CPC by species showed an increasing pattern in both species as the number of scans increased, with *Pk* increasing to 45%, 71%, 88%, 94%, and 99%, and *LK* increasing to 46%, 75%, 91%, 95%, and 98%. The stand densities for *PK* and *LK* were 925 and 390 trees/ha, respectively, with *PK* having approximately 2.3 times more trees. However, the average CPC of the two species varied by less than 5% depending on the number of scans, indicating a minor difference. As the number of scans increased, the standard deviation of the CPC in *PK* showed a pattern of increase and then decrease, with values of 8.14, 15.31, 12.93, 8.29, and 3.91, indicating an increase from one to three scans, followed by a decrease. Similarly, *LK* exhibited the same pattern with values of 6.59, 13.27, 9.99, 7.75, 5.28. However, compared to *PK*, *LK* had a lower standard deviation in one scan but a higher standard deviation in nine scans. Consequently, it was inferred that in *LK*, it was more challenging to construct a complete DBH point cloud than in *PK*. In areas with high stand density but low understory vegetation, increasing the number of scans enabled the construction of most of the information about stands in the PCD. However, in *LK*, where the understory vegetation obscured visibility, there were limitations to constructing a complete DBH point cloud, even with an increased number of scans. In summary, for efficient scanning, it is appropriate to aim for approximately five scans, where the CPC reaches approximately 89%, beyond which the rate of increase decreases. Nine or more scans were necessary to obtain a complete point cloud (Figure 8).

Boxplots of the constructed factors and biases are shown in Figure 9. When the CPC was below 60%, the variance in the bias was significantly distributed, with ellipse fitting showing greater variance than circle fitting. When the CPC was above 60%, the bias between the different circular fitting algorithms was similarly distributed, and the bias decreased. Furthermore, as the CPC approached 100%, the bias and variance decreased, allowing for a more accurate estimation of diameter at breast height (DBH). Therefore, for consistent DBH estimation, the data collection must comprise at least 60% CPC, and it can be observed that the performance of DBH estimation is proportional to the CPC.

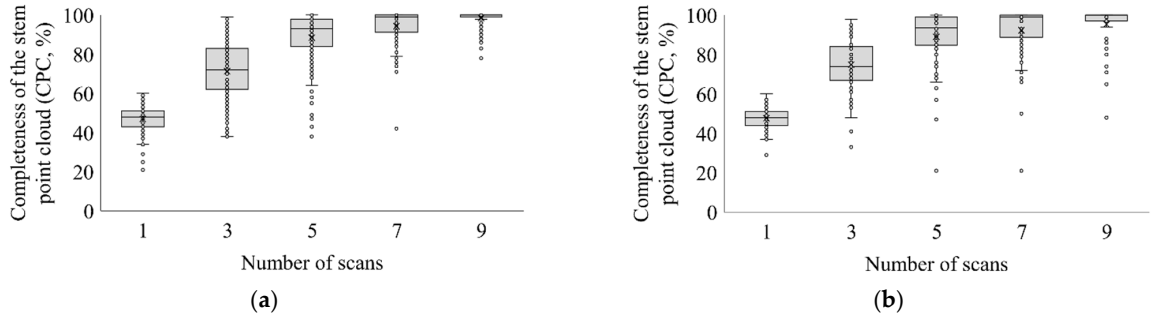

Figure 8. Result of calculated completeness of the stem point cloud depending on number of scans: (**a**) *PK*; (**b**) *LK*.

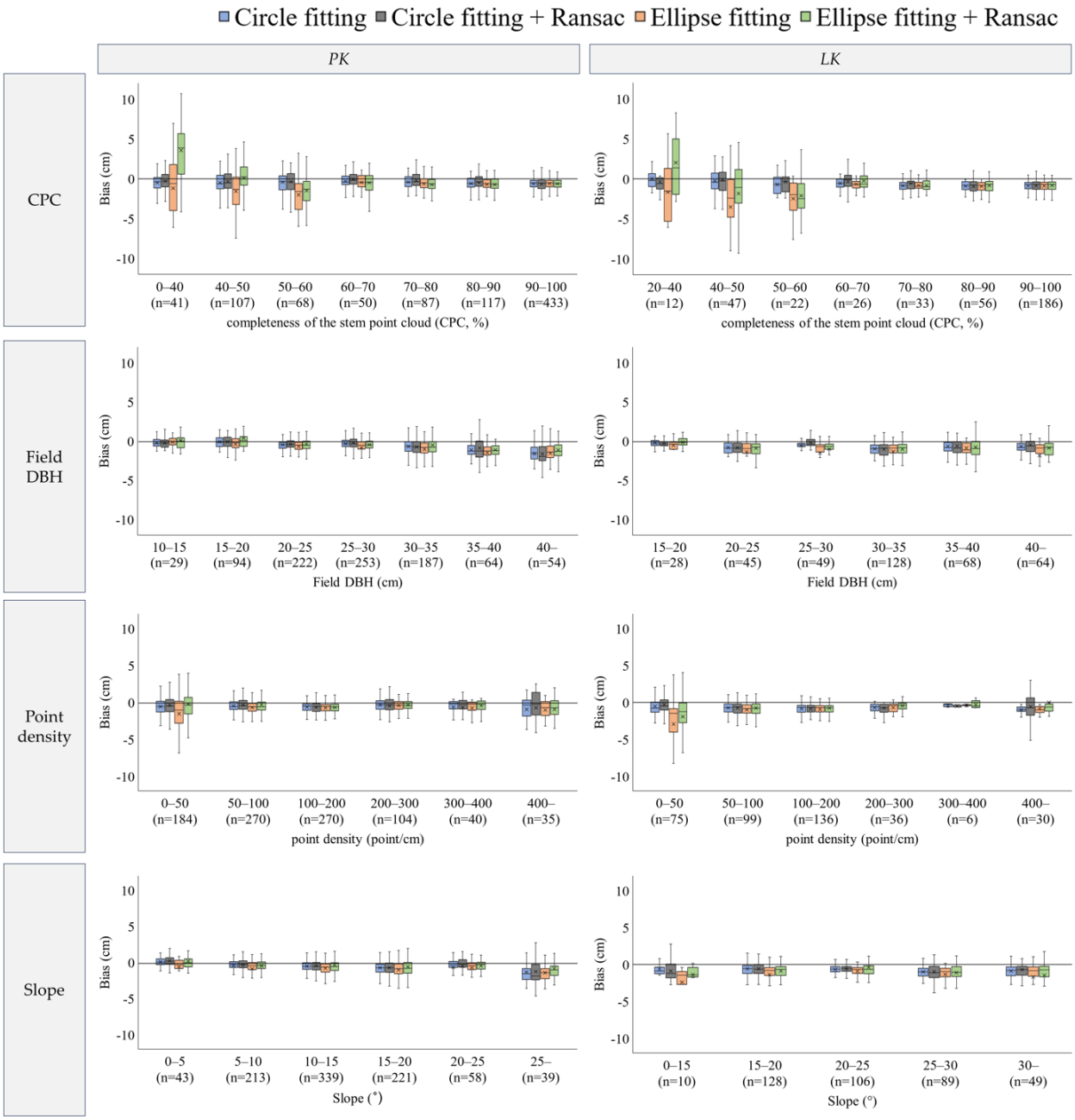

Figure 9. Boxplots of bias (Estimation DBH—Field DBH) depending on influencing factors, species, and fitting method using denoised data.

The relationship between Field DBH and bias showed that as Field DBH increased, the mean value of the bias gradually decreased, whereas the variance did not change significantly. In this study, Field DBH was measured using a diameter tape, and the results are consistent with those of previous studies that estimated and evaluated DBH using LiDAR systems and a diameter tape [35]. Diameter tape, a measuring tool designed based on the assumption of a circular shape, can result in overestimation when the cross-section of breast height is in the form of an ellipse or an irregular shape. Moreover, this error increases with DBH, even in ellipses with the same eccentricity [6]. Therefore, the underestimation of DBH using point cloud data in cases of larger-field DBH is considered to be a limitation inherent in the characteristics of the diameter tape, making it challenging to attribute this to errors in the LiDAR system.

The accuracy of estimating the DBH based on point density improved as the point density increased. However, at the highest point density levels exceeding 400 points, the accuracy decreased. Previous research related to point density and DBH estimation has indicated that lower point densities can lead to increased errors [40]. Additionally, when using MLS, it was observed that the error pattern initially decreased and then increased again with an increase in point density [35]. The point density varies owing to multiple factors, including the distance and angle from the scanner to the target, resolution of the equipment, slope, size of the target, and scanning settings. Additionally, in multi-scan scenarios, the point density can vary depending on the number and position of the scans [41]. Therefore, errors arising from the specifications of the equipment and alignment process, particularly in multi-scan scenarios with high point density, need to be considered.

The slope influenced the accuracy of the measurements, with the bias variance increasing and the accuracy decreasing as the slope exceeded 15°. The slope affects the extraction of ground points and the construction of the DEM. According to previous research, higher slopes are associated with significant errors in the DEM [42]. Ground points and DEM are crucial for estimating the forest resource parameters using LiDAR systems. In this study, ground points were used to extract points at the breast height locations (1.15–1.25 m). As a result, the higher error in DBH estimation in larch forests than in pine forests can be partly attributed to steeper slopes. In the future, for accurate forest resource estimation using LiDAR systems, it will be necessary to review methods for extracting accurate ground points under various environmental conditions.

4. Conclusions

This study aimed to compare the accuracy of DBH estimation using terrestrial laser scanning (TLS) based on the number of scans and circular fitting algorithms. The number of scans was set to 1, 3, 5, 7, and 9 to construct the point cloud at the plot level, and ground points were extracted to establish points at breast height. DBH was measured using CF, RCF, EF, and REF applied to the constructed breast height points, and the optimal number of scans was determined using ANOVA. Additionally, each tree's CPC, Field DBH, point density, and slope information were constructed as influencing factors for DBH estimation, and their relationships with bias were analyzed.

The number of scans in the TLS was proportional to the accuracy; however, the increase in accuracy gradually diminished. However, excessive scanning can lead to reduced accuracy due to scanner limitations, cumulative errors in the alignment process, and scanning noise from understory vegetation and branches. Particularly, in a single scan, more than 90% of individual trees could be estimated for DBH, and in five scans, the identification of all individual trees was possible. Statistical analysis showed no significant difference in bias between the data from the nine scans and three or more scans. Thus, considering the increasing cost of data collection and preprocessing with more scans, a careful selection of the number of scans is necessary based on these results.

The optimal circular fitting algorithm varied depending on the number of scans and presence of data noise. CF allowed for a more accurate DBH estimation with fewer scans and a lower CPC than EF. The EF performed better with higher scan counts and complete

data collection. The effectiveness of the RANSAC algorithm for data with noisy points, such as understory vegetation, was also clearly observed. Therefore, selecting a circular fitting algorithm based on site and data collection status can enable effective DBH estimation.

Finally, when evaluating the main factors affecting DBH estimation, it was found that the variance in bias decreased when the CPC was above 60%, and as Field DBH increased, the DBH estimated using LiDAR was underestimated. However, this underestimation is considered to be a result of the overmeasurement of Field DBH in large trees owing to the characteristics of the diameter tape. Therefore, when evaluating data collected using LiDAR, it is necessary to consider the characteristics of the conventional measuring equipment. Finally, as the point density increased, the accuracy increased until it reached 400 points/cm, after which it decreased. Hence, for accurate and precise DBH estimation, data collection and preprocessing must be conducted to maintain an appropriate level of point density.

This study examined the variations in accuracy depending on the data construction methods centered around DBH. Recently, research using LiDAR systems to estimate various forest-related parameters such as tree height, biomass, forest structure, and 3D modeling was conducted [43–47]. Therefore, future research should not only explore DBH but also how data construction methods influence the estimation of various forest parameters.

Author Contributions: Conceptualization, Y.L. and J.L.; methodology, Y.L. and J.L.; software, Y.L.; validation, Y.L. and J.L.; formal analysis, Y.L.; investigation, Y.L.; resources, Y.L.; data curation, Y.L.; writing—original draft preparation, Y.L.; writing—review and editing, J.L.; visualization, Y.L.; supervision, J.L.; project administration, J.L.; funding acquisition, J.L. All authors have read and agreed to the published version of the manuscript.

Funding: This research was funded by the Korea Forestry Service (Korea Forestry Promotion Institute), 2019151D10-2323-0301 and 2021359A00-2223-BD01.

Data Availability Statement: The data presented in this study are available on request from the corresponding author.

Conflicts of Interest: The authors declare no conflicts of interest.

References

1. Yim, J.S.; Kim, D.H.; Ko, C.U.; Kim, D.G.; Cho, H.J. Design and Implementation of System for Estimating Diameter at Breast Height and Tree Height using LiDAR point cloud data. *JKSCI* **2023**, *28*, 99–110.
2. McTague, J.P.; Weiskittel, A. Evolution, history, and use of stem taper equations: A review of their development, application, and implementation. *Can. J. For. Res.* **2021**, *51*, 210–235. [CrossRef]
3. Chen, J.; Yang, H.; Man, R.; Wang, W.; Sharma, M.; Peng, C.; Parton, J.; Zhu, H.; Deng, Z. Using machine learning to synthesize spatiotemporal data for modelling DBH-height and DBH-height-age relationships in boreal forests. *For. Ecol. Manag.* **2020**, *466*, 118104. [CrossRef]
4. Semenzato, P.; Cattaneo, D.; Dainese, M. Growth prediction for five tree species in an Italian urban forest. *Urban For. Urban Green.* **2011**, *10*, 169–176. [CrossRef]
5. Brokaw, N.; Thompson, J. The H for DBH. *For. Ecol. Manag.* **2000**, *129*, 89–91. [CrossRef]
6. Binot, J.M.; Pothier, D.; Lebel, J. Comparison of relative accuracy and time requirement between the caliper, the diameter tape and an electronic tree measuring fork. *For. Chron.* **1995**, *71*, 197–200. [CrossRef]
7. McRoberts, R.E.; Hahn, J.T.; Hefty, G.J.; Cleve, J.R.V. Variation in forest inventory field measurements. *Can. J. For. Res.* **1994**, *24*, 1766–1770. [CrossRef]
8. Zhang, W.; Ke, Y.; Quackenbush, L.J.; Zhang, L. Using error-in-variable regression to predict tree diameter and crown width from remotely sensed imagery. *Can. J. For. Res.* **2010**, *40*, 1095–1108. [CrossRef]
9. Kattenborn, T.; Hernández, J.; Lopatin, J.; Kattenborn, G.; Fassnacht, F.E. Pilot study on the retrieval of DBH and diameter distribution of deciduous forest stands using cast shadows in uav-based orthomosaics. *ISPRS Ann.* **2018**, *4*, 93–99.
10. Pitkänen, T.P.; Raumonen, P.; Kangas, A. Measuring stem diameters with TLS in boreal forests by complementary fitting procedure. *ISPRS J. Photogramm. Remote Sens.* **2019**, *147*, 294–306. [CrossRef]
11. Donager, J.J.; Sánchez Meador, A.J.; Blackburn, R.C. Adjudicating perspectives on forest structure: How do airborne, terrestrial, and mobile Lidar-derived estimates compare? *Remote Sens.* **2021**, *13*, 2297. [CrossRef]
12. Holopainen, M.; Kankare, V.; Vastaranta, M.; Liang, X.; Lin, Y.; Vaaja, M.; Yu, X.; Hyyppä, J.; Hyyppä, H.; Kaartinen, H. Tree mapping using airborne, terrestrial and mobile laser scanning—A case study in a heterogeneous urban forest. *Urban For. Urban Green.* **2013**, *12*, 546–553. [CrossRef]

13. Liu, G.; Wang, J.; Dong, P.; Chen, Y.; Liu, Z. Estimating Individual Tree Height and Diameter at Breast Height (DBH) from Terrestrial Laser Scanning (TLS) Data at Plot Level. *Forests.* **2018**, *9*, 398. [CrossRef]
14. Singh, A.; Kushwaha, S.K.P.; Nandy, S.; Padalia, H. An approach for tree volume estimation using RANSAC and RHT algorithms from TLS dataset. *Appl. Geomat.* **2022**, *14*, 785–794. [CrossRef]
15. Ritter, T.; Schwarz, M.; Tockner, A.; Leisch, F.; Nothdurft, A. Automatic Mapping of Forest Stands Based on Three-Dimensional Point Clouds Derived from Terrestrial Laser-Scanning. *Forests* **2017**, *8*, 265. [CrossRef]
16. Liu, C.; Xing, Y.; Duanmu, J.; Tian, X. Evaluating different methods for estimating diameter at breast height from terrestrial laser scanning. *Remote Sens.* **2018**, *10*, 513. [CrossRef]
17. Koreň, M.; Mokroš, M.; Bucha, T. Accuracy of tree diameter estimation from terrestrial laser scanning by circle-fitting methods. *Int. J. Appl. Earth Obs. Geoinf.* **2017**, *63*, 122–128. [CrossRef]
18. Kong, J.; Ding, X.; Liu, J.; Yan, L.; Wang, J. New hybrid algorithms for estimating tree stem diameters at breast height using a two dimensional terrestrial laser scanner. *Sensors* **2015**, *15*, 15661–15683. [CrossRef]
19. Zhou, J.; Zhou, G.; Wei, H.; Zhang, X.; Wang, X. Evaluation of three methods for estimating diameter at breast height from terrestrial laser scanning data. In Proceedings of the IGARSS 2019-2019 IEEE International Geoscience and Remote Sensing Symposium, Yokohama, Japan, 28 July–2 August 2019; pp. 6674–6677.
20. Olofsson, K.; Holmgren, J.; Olsson, H. Tree Stem and Height Measurements using Terrestrial Laser Scanning and the RANSAC Algorithm. *Remote Sens.* **2014**, *6*, 4323–4344. [CrossRef]
21. Torralba, J.; Carbonell-Rivera, J.P.; Ruiz, L.Á.; Crespo-Peremarch, P. Analyzing TLS scan distribution and point density for the estimation of forest stand structural parameters. *Forests* **2022**, *13*, 2115. [CrossRef]
22. Wang, Y.; Lehtomäki, M.; Liang, X.; Pyörälä, J.; Kukko, A.; Jaakkola, A.; Liu, J.; Feng, Z.; Chen, R.; Hyyppä, J. Is field-measured tree height as reliable as believed—A comparison study of tree height estimates from field measurement, airborne laser scanning and terrestrial laser scanning in a boreal forest. *ISPRS J. Photogramm. Remote Sens.* **2019**, *147*, 132–145. [CrossRef]
23. Cabo, C.; Ordóñez, C.; López-Sánchez, C.A.; Armesto, J. Automatic dendrometry: Tree detection, tree height, and diameter estimation using terrestrial laser scanning. *Int. J. Appl. Earth Obs. Geoinf.* **2018**, *69*, 164–174. [CrossRef]
24. Liang, X.; Litkey, P.; Hyyppa, J.; Kaartinen, H.; Vastaranta, M.; Holopainen, M. Automatic Stem Mapping Using Single-Scan Terrestrial Laser Scanning. *IEEE Trans. Geosci. Remote Sens.* **2011**, *50*, 661–670. [CrossRef]
25. Lee, Y.K.; Son, Y.W.; Oh, J.S. Effects of Nitrogen and Phosphorus Fertilization on Aboveground Biomass and Distribution of Nutrient Content of Pinus rigida and Larix kaempferi Plantations in Yangpyeong area, Gyeonggi Province. *J. Korea For. Energy* **2004**, *23*, 1–18.
26. Korea Forest Service. *The 8th National Forest Inventory and Forest Health Monitoring—Field Manual*; Korea Forest Service: Daejeon, Republic of Korea, 2021; p. 37.
27. Pokswinski, S.; Gallagher, M.R.; Skowronski, N.S.; Loudermilk, E.L.; Hawley, C.; Wallace, D.; Everland, A.; Wallace, J.; Hiers, J.K. A simplified and affordable approach to forest monitoring using single terrestrial laser scans and transect sampling. *MethodsX* **2021**, *8*, 101484. [CrossRef] [PubMed]
28. Calders, K.; Adams, J.; Armston, J.; Bartholomeus, H.; Bauwens, S.; Bentley, L.P.; Chave, J.; Danson, F.M.; Demol, M.; Disney, M. Terrestrial laser scanning in forest ecology: Expanding the horizon. *Remote Sens. Environ.* **2020**, *251*, 112102. [CrossRef]
29. Zhang, W.; Qi, J.; Wan, P.; Wang, H.; Xie, D.; Wang, X.; Yan, G. An Easy-to-Use Airborne LiDAR Data Filtering Method Based on Cloth Simulation. *Remote Sens.* **2016**, *8*, 501. [CrossRef]
30. Fareed, N.; Flores, J.P.; Das, A.K. Analysis of UAS-LiDAR Ground Points Classification in Agricultural Fields Using Traditional Algorithms and PointCNN. *Forests* **2023**, *15*, 483. [CrossRef]
31. Heinzel, J.; Huber, M.O. Detecting tree stems from volumetric TLS data in forest environments with rich understory. *Remote Sens.* **2016**, *9*, 9. [CrossRef]
32. Wang, F.; Heenkenda, M.K.; Freeburn, J.T. Estimating tree diameter at breast height (DBH) using an iPad Pro LiDAR Sensor. *Remote Sens. Lett.* **2022**, *13*, 568–578. [CrossRef]
33. Gander, W.; Golub, G.H.; Strebel, R. Least-squares fitting of circles and ellipses. *BIT Numer. Math.* **1994**, *34*, 558–578. [CrossRef]
34. Fischler, M.A.; Bolles, R.C. Random sample consensus: A paradigm for model fitting with applications to image analysis and automated cartography. *Commun. ACM* **1981**, *24*, 381–395. [CrossRef]
35. Xie, Y.; Yang, T.; Wang, X.; Chen, X.; Pang, S.; Hu, J.; Wang, A.; Chen, L.; Shen, Z. Applying a Portable Backpack Lidar to Measure and Locate Trees in a Nature Forest Plot Accuracy and Error Analyses. *Remote Sens.* **2022**, *14*, 1806. [CrossRef]
36. Xie, Y.; Zhang, J.; Chen, X.; Pang, S.; Zeng, H.; Shen, Z. Accuracy assessment and error analysis for diameter at breast height measurement of trees obtained using a novel backpack LiDAR system. *For. Ecosyst.* **2020**, *7*, 33. [CrossRef]
37. Mokros, M.; Mikita, T.; Singh, A.; Tomaštík, J.; Chudá, J.; Wężyk, P.; Kuželka, K.; Surový, P.; Klimánek, M.; Zięba-Kulawik, K.; et al. Novel low-cost mobile mapping systems for forest inventories as terrestrial laser scanning alternatives. *Int. J. Appl. Earth Obs. Geoinf.* **2021**, *104*, 102512.
38. Panagiotidis, D.; Abdollahnejad, A.; Slavik, M. 3D point cloud fusion from UAV and TLS to assess temperate managed forest structures. *Int. J. Appl. Earth Obs. Geoinf.* **2022**, *112*, 102917. [CrossRef]
39. Ruhan, A.; Du, W.; Ying, H.; Wei, B.; Shan, Y.; Dai, H. Estimation of Aboveground Biomass of Individual Trees by Backpack LiDAR Based on Parameter-Optimized Quantitative Structural Models (AdQSM). *Forests* **2023**, *14*, 475. [CrossRef]

40. Srinivasan, S.; Popescu, S.C.; Eriksson, M.; Sheridan, R.D.; Ku, N.W. Terrestrial Laser Scanning as an Effective Tool to Retrieve Tree Level Height, Crown Width, and Stem Diameter. *Remote Sens.* **2015**, *7*, 1877–1896. [CrossRef]
41. Liu, S.; Tan, K.; Tao, P.; Yang, J.; Zhang, W.; Wang, Y. Rigorous Density Correction Model for Single-Scan TLS Point Clouds. *IEEE Trans. Geosci. Remote Sens.* **2023**, *61*, 5701318. [CrossRef]
42. Bauwens, S.; Bartholomeus, H.; Calders, K.; Lejeune, P. Forest Inventory with Terrestrial LiDAR: A Comparison of Static and Hand-Held Mobile Laser Scanning. *Forests* **2016**, *7*, 127. [CrossRef]
43. Du, S.; Lindenbergh, R.; Ledoux, H.; Stoter, J.; Nan, L. AdTree: Accurate, detailed, and Automatic Modelling of Laser-Scanned Trees. *Remote Sens.* **2019**, *11*, 2074. [CrossRef]
44. Raumonen, P.; Kaasalainen, M.; Åkerblom, M.; Kaasalainen, S.; Kaartinen, H.; Vastaranta, M.; Holopainen, M.; Disney, M.; Lewis, P. Fast Automatic Precision Tree Models from Terrestrial Laser Scanner Data. *Remote Sens.* **2013**, *5*, 491–520. [CrossRef]
45. Delagrange, S.; Jauvin, C.; Rochon, P. PypeTree: A Tool for Reconstructing Tree Perennial Tissues from Point Clouds. *Sensors* **2014**, *14*, 4271–4289. [CrossRef] [PubMed]
46. Wang, F.; Sun, Y.; Jia, W.; Li, D.; Zhang, X.; Tang, Y.; Guo, H. A Novel Approach to Characterizing Crown Vertical Profile Shapes using Terrestrial Laser Scanning (TLS). *Remote Sens.* **2023**, *15*, 3272. [CrossRef]
47. Wang, F.; Sun, Y.; Jia, W.; Zhu, W.; Li, D.; Zhang, X.; Tang, Y.; Guo, H. Development of estimation models for individual tree aboveground biomass based on TLS-derived parameters. *Forests* **2023**, *14*, 351. [CrossRef]